In Vivo Clearance and Toxicity of Monodisperse Iron Oxide Nanocrystals

Luo Gu,[†] Ronnie H. Fang,[∥] Michael J. Sailor,[†,‡,§] and Ji-Ho Park[⊥,*]

[†]Department of Chemistry and Biochemistry, [∥]Department of Nanoengineering, [‡]Department of Bioengineering, and [§]Materials Science and Engineering Program, University of California, San Diego, La Jolla, California 92093, United States, and [⊥]Department of Bio and Brain Engineering, Korea Advanced Institute of Science and Technology, Daejeon, 305-701, Republic of Korea

ABSTRACT

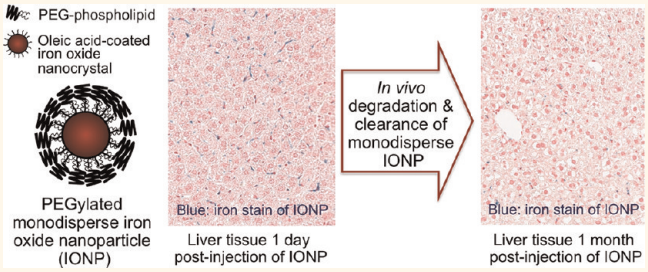

Thermal decomposition of organometallic precursors has been found to generate highly crystalline iron oxide (IO) nanocrystals that display superior MR contrast and lower polydispersity than IO nanocrystals synthesized by aqueous precipitation. In the present study, the *in vivo* characteristics of IO nanocrystals prepared by the thermal decomposition route and then coated with a phospholipid containing a pendant poly(ethylene glycol) chain are examined. The size and surface chemistry of the IO nanocrystal influence the biodistribution, the rate of biodegradation and bioclearance, and the biodegradation products. We conclude that the *in vivo* fate of PEGylated monodisperse IO nanocrystals and the iron, phospholipid, and oleic acid biodegradation products may influence the cellular environments in the organs and blood that can determine their safety in the body.

KEYWORDS: iron oxide nanoparticle · biodistribution · biodegradation · bioclearance · biocompatibility

Magnetic iron oxide (IO) nanoparticles are used in a range of biomedical applications: hyperthermia, magnetically targeted delivery, and particularly molecular magnetic resonance imaging (MRI) diagnosis.[1,2] The superparamagnetism of IO nanoparticles decreases the spin−spin relaxation time of surrounding water protons, enhancing the contrast in T_2-weighted MR images.[3] Several types of systemically administered IO nanoparticle contrast agents have been approved for human use by the U.S. Food and Drug Administration (FDA). For example, Feridex is a dextran-coated cluster of IO nanoparticles approved as a contrast agent for hepatic imaging.[4] Conventional preparation of such nanoparticles involves co-precipitation of iron(II) and iron(III) salts from an aqueous solution containing dextran molecules.

Recently, monodisperse and highly crystalline IO nanocrystals that show superior MR imaging characteristics have been synthesized by high-temperature decomposition of organometallic iron precursors in organic solvents.[5−8] This synthetic approach provides excellent control of size, shape, stoichiometry, and magnetism.[9,10] In addition, the method provides a means to incorporate various additional elements (*e.g.*, Mn, Co, and Zn) into the lattice.[11,12] However, the synthesis generates a layer of hydrophobic molecules attached to the surface of the nanocrystals that must be replaced or coated to impart water solubility to the nanoparticles.[12−15] One of the most popular and biocompatible coating materials is a polyethylene glycol (PEG)-terminated phospholipid.[16,17] The hydrocarbon chain of this FDA-approved phospholipid adsorbs to the capping molecules on the nanocrystal surface *via* hydrophobic van der Waals interactions, while the outer PEG chain allows the nanocrystal to be dispersed and well suspended in biological solutions and to circulate in the bloodstream for a relatively long time.[18]

To be used as a MRI contrast agent, the IO nanoparticles must be administered systemically. Most nanoparticles introduced to the bloodstream are taken up by the organs of the mononuclear phagocytic system (MPS) such as the liver and the spleen. In order to ensure biosafety, it is important to evaluate the long-term biodistribution, biodegradation, and bioclearance of IO nanoparticles introduced to the body.[4,19,20] It is known that IO nanoparticles are taken up in the MPS *via* endocytosis into Kupffer cells of the liver sinusoid and macrophages of the splenic red pulp, where they are then degraded in the lysosomes of those cells.

* Address correspondence to jihopark@kaist.ac.kr.

Received for review January 31, 2012 and accepted May 30, 2012.

Published online May 30, 2012
10.1021/nn300456z

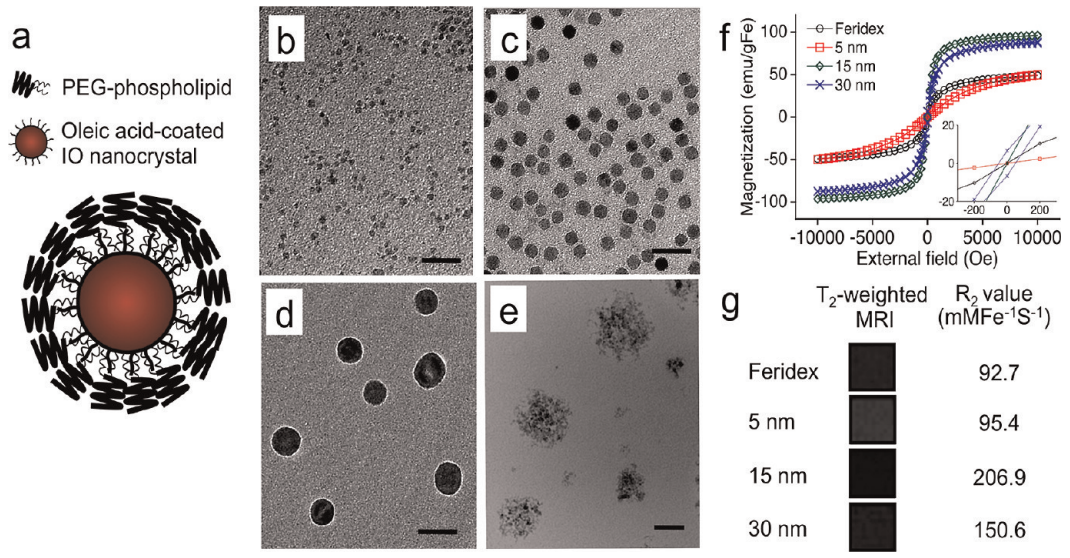

Figure 1. Physical characteristics of iron oxide (IO) nanoparticles. (a) Schematic representation of a monodisperse IO nanocrystal prepared *via* the organometallic route and then coated with amphiphilic PEG-phospholipids. (b−d) Transmission electron microscope (TEM) images of PEG-phospholipid-coated IO nanocrystals; average sizes ~5 nm (b), ~15 nm (c), and ~30 nm (d). (e) TEM image of commercial Feridex IO nanoparticle preparation for comparison. Scale bar is 50 nm for images b−e. (f) Room-temperature magnetization curves comparing monodisperse IO nanocrystal preparations and Feridex. Inset shows an expansion of the region near 0 T. (g) T_2-weighted magnetic resonance images and relaxivity R_2 values of monodisperse IO nanocrystals and Feridex.

The degraded iron is finally eliminated from or restored in the body *via* normal iron metabolic pathways.[19−21] Although the *in vivo* characteristics of (dextran-coated) IO nanoparticles prepared by aqueous precipitation have been well studied in many animal models,[19−22] biodistribution, biodegradation, and bioclearance of the monodisperse IO nanocrystals synthesized by the organometallic method have not been explored in detail. Previously, the long-term *in vivo* fate of pluronic triblock copolymer[14] or poly(D,L-lactic-*co*-glycolic acid)[15] nanoparticles (size >100 nm) containing multiple oleic acid-coated IO nanocrystals (each of size ≈ 10 nm) has been tested. Because they do not employ isolated IO nanocrystals, these larger composite structures do not capitalize on the excellent monodispersity of the organometallic preparation.

The factors determining the biosafety of monodisperse nanocrystals in the body must be systematically studied in order to enable clinical translation. In the present study, we assess *in vivo* characteristics (MR contrast and blood residence time) of monodispersed PEGylgated IO nanocrystals in mice. We investigate the influence of size and surface chemistry on retention of the nanocrystals and the iron biodegradation products in various collecting organs over a 30-day period. Furthermore, we investigate the interaction of the biodegradation products of the IO nanocrystals (iron complexes, phospholipids, and oleic acids) with the cellular environments of organs and blood.

RESULTS AND DISCUSSION

Monodisperse IO nanocrystals with average sizes of ~5, 15, and 30 nm were synthesized by thermolysis of iron precursors in an organic solvent following the published preparation.[5] The preparation results in nanocrystals containing a monolayer coating of oleic acid. In order to solubilize them in the aqueous media, the hydrophobic nanocrystals were encapsulated with PEG-phospholipids, forming a micellar nanostructure (Figure 1a). By transmission electron microscopy (TEM, Figure 1b−e), the PEGylated nanocrystals appear individually dispersed with relatively uniform diameters. In contrast, Feridex appears as clusters of 2−4 nm IO cores. The hydrodynamic diameters, measured by dynamic light scattering, were 153.0 ± 11.9, 13.3 ± 1.8, 28.7 ± 3.2, and 52.1 ± 2.5 nm for Feridex and 5, 15, and 30 nm IO nanocrystals, respectively. These values are somewhat larger than those observed in the TEM images due to the organic coating layer (PEG for monodisperse IO nanocrystals and dextran for Feridex). No aggregation was observed for all formulations after 3 months of storage in PBS buffer at 4 °C.

The magnetic behavior of the IO nanoparticles was examined using a superconducting quantum interference device (SQUID, Figure 1f). The magnetization increased with increasing nanocrystal size, consistent with the previous report,[9] although the 15 and 30 nm nanocrystal formulations did not show significant differences in magnetization. In addition, the magnetization curve of the 30 nm nanocrystal formulation displayed a discernible hysteresis loop, indicating the onset of ferrimagnetism in this largest nanoparticle of the study. Magnetic nanoparticles with ferrimagnetic and ferromagnetic characteristics are less desirable than superparamagnetic formulations for MRI applications due to their lower contrast.[3] In the MR

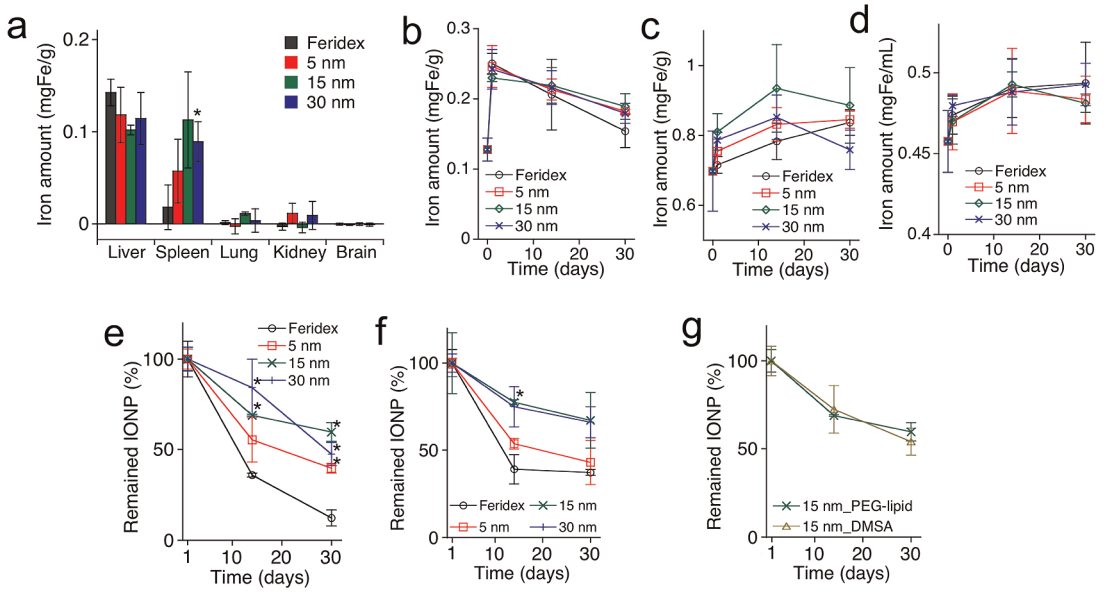

Figure 2. ***In vivo*** **accumulation, degradation, and clearance of iron oxide (IO) nanoparticles in mice. (a) Excess iron accumulated in the indicated organs 24 h after intravenous injection (5 mgFe/kg) of PEG–phospholipid-coated IO nanocrystals, prepared** ***via*** **the organometallic route (sizes of ~5, ~15, and ~30 nm), and Feridex. Excess iron accumulated in the organs relative to PBS control injection, quantified by ICP-OES. (b–d) Quantity of total iron (measured by ICP-OES) in liver (b), spleen (c), and blood (d) as a function of days after intravenous injection (5 mgFe/kg). Data point at day 0 represents the quantity of iron in the organs preinjection. (e and f) Percent of IO nanoparticles (percent superparamagnetic/ferrimagnetic content, measured by SQUID) remaining in liver (e) and spleen (f) as a function of days after intravenous injection (5 mgFe/kg). Data point at day 1 represents organs obtained 24 h postinjection. (g) Percent of IO nanoparticles (percent superparamagnetic/ferrimagnetic content, measured by SQUID) remaining in liver as a function of days after intravenous injection (5 mgFe/kg). Two different surface coatings, PEG-phospholipid and DMSA, are compared. Statistical analyses were performed with Student's** ***t*** **test (*$p < 0.05$ for the difference between monodisperse IO nanoparticles and Feridex nanoparticles, two-tailed, unpaired, $n = 4–6$, error bars = standard deviation).**

measurements (Figure 1g), the 15 nm nanocrystals exhibited the greatest contrast (based on iron mass) relative to other formulations. This is attributed to their superparamagnetic nature and their large mass magnetization values.[3,9]

Consistent with prior reports, HeLa cells treated with all the organometallic nanoparticle formulations studied showed no statistically significant dose-related changes of cell viabilities (Supplementary Figure 1).[12,23] However, the *in vitro* results are primarily a reflection of the low toxicity of the surface chemistry (PEG and dextran) since the nanoparticles are not degraded within the time scale of the cellular assay (48 h).

We next observed the *in vivo* accumulation, degradation, and clearance of the IO nanoparticle formulations in mice. The 5 nm nanocrystals circulated longer in the bloodstream than the larger nanoparticles ($T_{1/2}$ = 44.9 ± 12.9, 201.5 ± 82.4, 82.4 ± 8.3, and 62.8 ± 3.4 min for Feridex and 5, 15, and 30 nm nanocrystals, respectively), which is in agreement with previous findings.[24,25] The PEG layer on the nanocrystal surface apparently prolongs their blood residence time. The biodistribution of iron, obtained 24 h postinjection using inductively coupled plasma optical emission spectroscopy (ICP-OES), showed that the nanoparticles mainly accumulated in the MPS organs (liver and spleen, Figure 2a).[10,12,26] The Feridex nanoparticles showed less uptake in the spleen than the other formulations. Only minimal quantities of nanoparticles were detectable in other organs, such as brain, kidney, and lung.

Previous studies have established that systemically administered IO nanoparticles prepared by the aqueous route accumulate in the liver and spleen and are then degraded and excreted into the bloodstream in various monatomic iron forms. These ferrous Fe(II) and ferric Fe(III) degradation products then become incorporated into the hemoglobin of erythrocytes and into various iron-binding proteins and chelates (ferritin and transferrin).[19,20] We examined biodegradation and bioclearance of the organometallic IO nanoparticles in the liver and spleen and excretion of their degradation products into systemic circulation using ICP-OES (Figure 2b–d) and SQUID (Figure 2e and f) methods. The ICP-OES measurements were used to determine total quantity of iron, and the SQUID measurements yielded crystallinity and superparamagnetism data on intact IO cores. The SQUID data are dependent on the extent of both clearance and degradation of the IO cores; the Fe(II) and ferric Fe (III) degradation products do not provide a significant contribution to the superparamagnetism signal in the SQUID. For all IO nanoparticle formulations, the total mass of iron accumulated in the liver decreased with time, while the total mass of iron in the spleen was constant or slightly increased. In addition, the total mass of iron in the

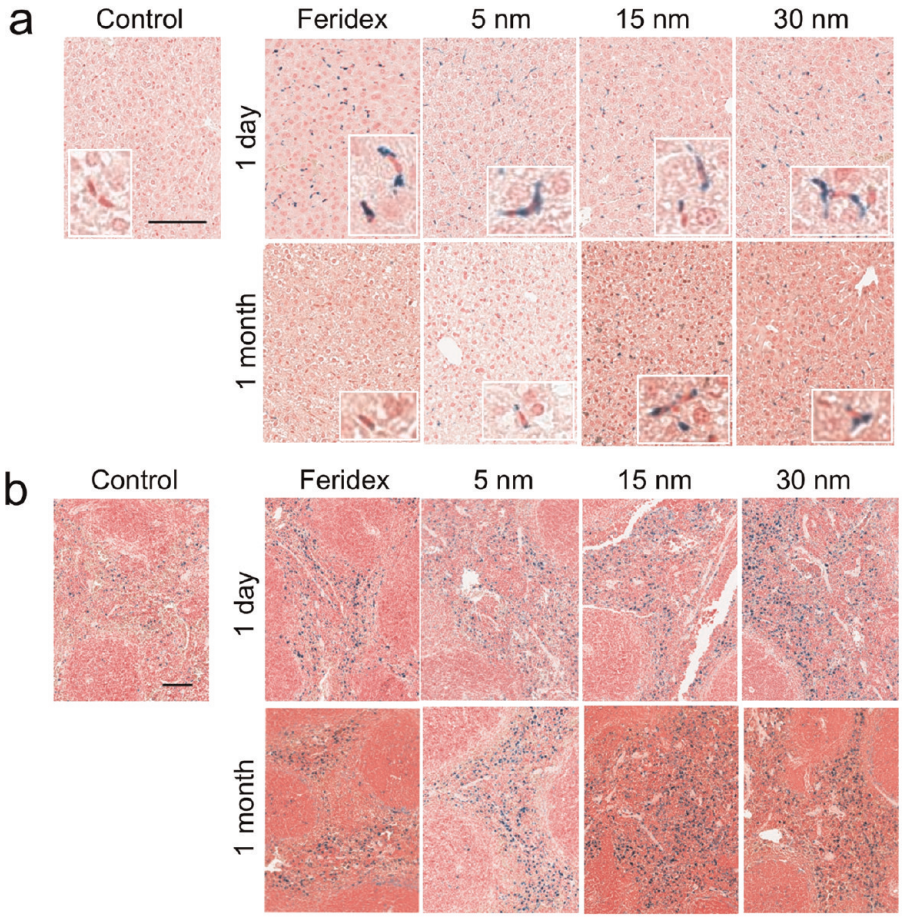

Figure 3. Histological sections showing distribution, degradation, and clearance of iron oxide (IO) nanoparticles in the liver and spleen. Monodisperse IO nanocrystals, prepared *via* the organometallic route and coated with PEG-phospholipid with sizes of ~5, ~15, and ~30 nm (as indicated), or Feridex was intravenously injected into mice at a dose of 5 mgFe/kg, and the sections of liver (a) and spleen (b) tissues harvested from the mice 1 day and 1 month after injection were processed with Prussian blue and nuclear fast red staining. The control samples were tissues from animals that were not injected with nanoparticles. The scale bar indicates 100 μm. The insets in (a) indicate the magnified images showing the Kupffer cells.

blood after nanoparticle injection was observed to slightly increase over time. In the SQUID measurements, the intensity of magnetization decreased over time in both the liver and the spleen, consistent with both degradation and clearance of the superparamagnetic IO cores. The ICP-OES and SQUID data for the spleen suggest that a large quantity of iron-containing degradation products from the IO nanoparticles was stored in the spleen. The increased concentration of total iron in the blood is attributed to the incorporation of iron from IO nanoparticle degradation into iron-associated proteins in the blood. Feridex displayed the largest rate of degradation and clearance in both liver and spleen compared to other formulations (measured over a 1-month period). The 5 nm nanocrystals exhibited somewhat faster degradation and clearance relative to the 15 and 30 nm nanocrystals. The dimercaptosuccinic acid (DMSA)-coated 15 nm nanocrystals (where the hydrophobic capping layer was partially replaced with hydrophilic DMSA molecules *via* a ligand exchange method[9,27]) showed rates of degradation and clearance in the liver similar to the PEG-phospholipid-coated nanocrystals (Figure 2g). These results indicate that the size and crystallinity of the IO cores (as shown by the TEM images of Figure 1b–e) are important factors determining the rate of biodegradation and bioclearance. However, it should be noted that replacement of the oleic acid surface coating with hydrophilic molecules is also expected to play a role in the rate of degradation *in vivo*.

Histology samples were also examined by Prussian blue staining (iron) to observe time-dependent degradation and clearance of the nanoparticles accumulated in the liver and spleen (Figure 3). Particularly, in the liver, most of the nanoparticles were found in the Kupffer cells located in the linings of the sinusoids, not in the hepatocytes, as observed in the magnified images. The iron staining of monodisperse nanocrystals in the tissues appeared somewhat weaker than that of Feridex. Because the ICP-OES data indicate that comparable (liver) or greater (spleen) quantities of the organometallic IO nanoparticle formulations accumulate in the organs relative to Feridex, it is possible that the hydrophobic capping layer on the

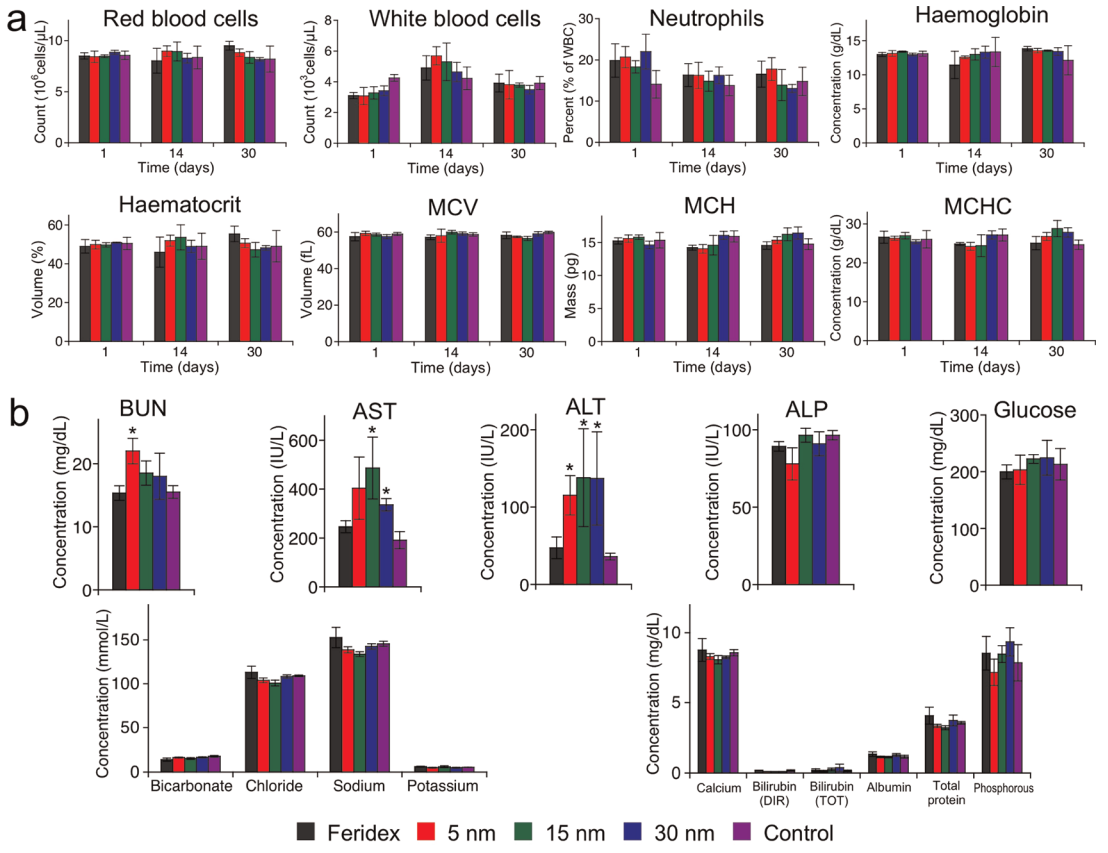

Figure 4. Hematology and blood chemistry of mice following injection of iron oxide (IO) nanoparticles, prepared *via* the organometallic route with sizes of ~5, ~15, or ~30 nm and coated with PEG-phospholipid, or commercially obtained Feridex (as indicated). (a) Red blood cell number, white blood cell number, percentage of neutrophils among white blood cells, hemoglobin concentration, hematocrit, mean corpuscular volume (MCV), mean corpuscular hemoglobin (MCH), and mean corpuscular hemoglobin concentration (MCHC) of mice 1, 14, and 30 days after intravenous injection with IO nanoparticles (5 mgFe/kg). (b) Concentration of blood urea nitrogen (BUN), aspartate transaminase (AST), alanine transaminase (ALT), alkaline phosphatase (ALP), glucose, bicarbonate, chloride, sodium, potassium, calcium, direct bilirubin (DIR), total bilirubin (TOT), albumin, total protein, and phosphorus of mice 30 days after intravenous injection with IO nanoparticles (5 mgFe/kg). Statistical analyses were performed with Student's *t* test (*$p < 0.05$ for the difference between IO nanoparticles and PBS, two-tailed, unpaired, $n = 4–6$, error bars = standard deviation).

organometallic IO nanoparticles impedes the reaction of ferrocyanide with ferric ion on the nanocrystal surface. At 1 month postinjection, no and minimal staining was observed in the liver injected with Feridex and 5 nm IO nanoparticles, respectively, while significant staining was observed in the livers of animals injected with either 15 or 30 nm nanocrystals. These results are consistent with the ICP-OES and SQUID data. In the spleen, similar degrees of iron staining were observed in both the 1-day and the 1-month postinjection samples for all IO nanoparticle formulations studied. As revealed by the ICP-OES data, significant quantities of iron degradation products appear to be stored in the spleen during degradation of the IO nanoparticles. This iron accumulation in the spleen could originate from ferritin stored in the macrophages, from phagocytosis of old red blood cells, or from remaining IO nanoparticles.

Body weights of mice injected with the nanoparticle formulations were monitored over a 1-month period postinjection and displayed no obvious losses due to the biodistribution, biodegradation, and bioclearance of the nanoparticles (Supplementary Figure 2). Additionally, histopathological examination (by a pathologist) of the liver and spleen tissues harvested 1 month postinjection yielded no significant signs of tissue damage (Supplementary Figure 3 shows organs stained with hematoxylin and eosin). Liver histology samples obtained 1 day postinjection showed some swollen and dark Kupffer cells, presumably due to uptake of the nanoparticles.

Since we observed significant quantities of the monodisperse nanocrystal formulations remaining in the liver and spleen 1 month postinjection, we searched for signs of *in vivo* toxicity with a complete set of hematology and blood chemistry assays (Figure 4). The hematology results showed the blood counts were within the normal range through the duration of the study, although there was a slight increase in the percentage of neutrophils 1 day postinjection, as would be expected from an immune reaction to foreign materials, here IO nanoparticles.

However, the neutrophil count returned to the normal (control) range within 1 month. The blood chemistry results showed increases in aspartate transaminase (AST) and alanine transaminase (ALT), enzymes mainly associated with the hepatocytes in the liver, in mice injected with the monodisperse IO formulations 1 month postinjection. Since the nanoparticles are first taken up in the Kupffer cells in the liver, it is suggested that the increase of AST and ALT levels is due to slow transfer of presumably toxic degradation products of the monodisperse IO nanoparticles (hydrophobic oleic acid, *etc.*) from the macrophages to the hepatocytes. All other blood parameters tested (blood urea nitrogen, alkaline phosphatase, glucose, biocarbonate, chloride, sodium, potassium, calcium bilrubin, albumin, total protein, phosphorus) were within normal ranges. These results are somewhat different from a previous study with large pluronic-coated IO nanocomposites tested in rats, where increased levels of AST and ALT returned to normal within 3 days postinjection.[14] This discrepancy could be due to the animal model (mouse *vs* rat) or to the specific IO nanocrystal preparation method. Although further systematic examinations are required to verify *in vivo* long-term toxicity of the monodisperse nanocrystals tested here, these results indicate that the slow rate of degradation and clearance and the unique degradation products may contribute to subclinical toxicity.

CONCLUSION

The highly crystalline IO nanocrystal composition that can be prepared *via* the organometallic route shows an increased MR signal and improved monodispersity relative to IO nanoparticles prepared *via* the aqueous synthesis. The material is attractive for *in vivo* applications, where the enhanced contrast observed could lead to lower overall doses required to image target tissues. In addition, the more precise control of size and shape may satisfy limitations imposed by the nanoenvironments of target disease sites (*e.g.*, porous vessels in a tumor, nephron filtration in the kidney, or blood−brain barrier penetration). While the longer *in vivo* residence time of the IO formulation prepared by the organometallic route may provide an advantage for the monitoring of disease, it also poses challenges associated with longer-term toxicity. Materials suitable for clinical translation will require optimization of degradation and clearance rate to match residence time with the imaging needs.

MATERIALS AND METHODS

Nanoparticle Preparation and Charaterization. For the micellar coating, 200 μL of oleic acid-coated monodisperse iron oxide (IO) nanocrystals (5, 15, and 30 nm, prepared using a previously reported method with slight modification[5]) in chloroform (2 mg/mL) was mixed in a glass vial with 200 μL of 1,2-dipalmitoyl-*sn*-glycero-3-phosphoethanolamine-*N*-[methoxy(polyethylene glycol)-2000] (PEG-PE or PEG-phospholipids, Avanti Polar Lipids, Inc., AL, USA) in chloroform (10 mg/mL). After complete evaporation of the chloroform, the dried film was hydrated by adding 2 mL of water at 70 °C, and the synthesis vessel was placed in an ultrasonic bath for 5 min to obtain an optically clear suspension. The suspension was then filtered through a 0.1 μm membrane, and the micellar IO nanocrystals were selectively collected by trapping on a magnetic column (Miltenyi Biotec, Bergisch Gladbach, Germany). The immobilized particles were rinsed with phosphate-buffered saline (PBS) three times. Empty micelles passing through the column were removed during this process. The micellar IO nanocrystals were eluted from the column after removal of the magnet, using 1 mL of PBS. The suspension was again filtered through a 0.1 μm membrane to remove any aggregates produced during this magnetic trap process. Feridex IO nanoparticles were obtained from Berlex. For the ligand exchange, 1 mL of oleic acid-coated monodisperse IO nanocrytals in chloroform (10 mg/mL) was mixed with 1 mL of dimercaptosuccinic acid (Sigma) in dimethyl sulfoxide (DMSO, Sigma, 20 mg/mL), and triethylamine (100 μL) was added. The mixture was shaken overnight, and the nanoparticles were transferred from chloroform to DMSO. After centrifugation, the precipitate was rinsed with ethanol three times and dispersed in 1 mL of ethanol. A 1 mL portion of DMSA in DMSO (20 mg/mL) was added again to the nanocrystal ethanol solution, and the whole process was repeated. The final precipitate was dispersed in deionized water. For TEM imaging, an aliquot of the IO nanoparticles dispersed in deionized water was dropped onto the carbon film covering a 300-mesh copper minigrid (Ted Pella, Inc., CA, USA), which was then gently wiped off after approximately 1 min and air-dried. TEM images were obtained using a JEOL 2000EX transmission electron microscope. For the hydrodynamic size measurement, an aliquot (50 μL) of a diluted solution of the IO nanoparticles was transferred into a quartz cuvette, and hydrodynamic size measurements were obtained using a Malvern (Worcestershire, UK) Zetasizer ZS90. The hydrodynamic size indicates the mean value resulting from three measurements of *z*-average diameters of the nanoparticles (mean size ± standard deviation). For the magnetic measurement, 100 μL of a solution of the IO nanoparticles (1 mgFe/mL) was frozen and lyophilized to dryness in gelatin capsules. The capsules were inserted into the middle of transparent plastic straws. The measurements were performed at 298 K using a Quantum Design (CA, USA) MPMS2 SQUID magnetometer. The samples were exposed to direct current magnetic fields in stepwise increments up to 1 tesla. Corrections were made for the diamagnetic contribution of the capsule and straw. For the MRI T_2 mapping measurements, T_2 images of the IO nanoparticles were taken on a Bruker 4.7 T magnet, 7 cm core (Karlsruhe, Germany). Samples were serially diluted with aqueous PBS in a 384-well plate, containing 95 μL total sample/well. A series of 32 images with multiples of 15 ms echo times and a TR of 3000 ms were acquired. T_2 maps were obtained for each well using the T_2 fit map plug-in in OsiriX imaging software. R_2 is longitudinal relaxation rate, equal to the reciprocal of the T_2 relaxation time ($R_2 = 1/T_2$), and it is calculated with a T_2-weighted MRI map.

Nanoparticle Toxicity *in Vitro*. For the cytotoxicity test, HeLa human cervical cancer cells were incubated with nanoparticles of different concentrations for 48 h and then rinsed with cell medium three times ($n = 4$ per group). The cytotoxicity of various formulations of the IO nanoparticles was evaluated using the MTT (3-(4,5-dimethylthiazol-2-yl)-2,5-diphenyltetrazolium bromide) assay (Invitrogen). Cell viability was expressed as the percentage of viable cells compared with controls (cells treated with PBS).

Nanoparticle Behavior and Clearance *in Vivo*. All animal work was performed in accordance with the institutional animal protocol

guidelines in place at the Sanford-Burnham Medical Research Institute, and it was reviewed and approved by the Institute's Animal Research Committee. To quantify blood half-life, IO nanoparticles in PBS (100 μL) were intravenously injected into wild-type BALB/c mice at a dose of 5 mgFe/kg (n = 4 per group). Heparinized capillary tubes (Fisher) were used to draw 80 μL of blood from the periorbital plexus of the same mouse under anesthesia at different times (30 min, 1 h, 2 h, 4 h, and 8 h) after intravenous injection. The mouse was anesthetized only for the duration of the blood draw. The extracted blood samples were immediately spun down at 5000 rpm for 1 min to collect 20 μL of serum. The iron concentration of the serum sample was analyzed using an iron assay kit (BioChain Institute, Inc.), and the blood half-life was calculated by fitting the absorbance data to a single-exponential equation using a one-compartment open pharmacokinetic model[28] (mean blood half-life $\pm$ standard deviation). To determine their biodistribution in the mouse, IO nanoparticles in PBS (100 μL) were intravenously injected into wild-type BALB/c mice at a dose of 5 mgFe/kg (n = 4–6 per group). The mice were sacrificed 24 h after injection by cardiac perfusion with PBS under anesthesia, and the liver, spleen, kidney, lung, and brain were collected. The organs were weighed and then digested in a solution of HNO_3 (0.5 mL, ~15.7 M) and H_2O_2 (0.1 mL, 30%) for 2 days. The iron concentration in the samples was determined using ICP-OES (Perkin-Elmer Optima 3000DV). To evaluate biodegradation and bioclearance in the mouse, IO nanoparticles in PBS (100 μL) were intravenously injected into wild-type BALB/c mice at a dose of 5 mgFe/kg (n = 4–6 per group). The organs (liver and spleen) and blood were collected 1 day, 14 days, and 30 days after injection and weighed. Organ and blood samples for day 0 were obtained from control mice that were not injected with the nanoparticle solution. To determine change of total iron concentration over time, the organs and blood were digested in a solution of HNO_3 (0.5 mL, ~15.7 M) and H_2O_2 (0.1 mL, 30%) for 2 days. The iron concentration in the samples was determined using ICP-OES. To determine direct degradation and elimination of iron oxide nanoparticles over time, the organs were frozen and lyophilized to dryness in gelatin capsules. The change of superparamagnetic properties in the tissue samples was analyzed at 150 K using a SQUID magnetometer. Corrections were made for the diamagnetic contribution of the capsule and straw. The magnetization value (at 2000 Oe) in the superparamagnetic curves of the tissue samples was compared to determine degradation of IO nanoparticles. The IO nanoparticles remaining in the organs over time were expressed as a percentage (%) of total mass of IO nanoparticles accumulated in the tissue 1 day postinjection. To observe nanoparticle distribution in the tissues (liver and spleen), the sections of liver and spleen tissues harvested from the mice 1 day and 4 weeks after injection were processed with Prussian blue and nuclear fast red staining.

Nanoparticle Toxicity *in Vivo*. For the *in vivo* toxicity studies, the mass of each mouse was monitored for 4 weeks after injection of IO nanoparticles (5 mgFe/kg) and compared with control mice (PBS-injected) (n = 4–6 per group). The sections of liver and spleen tissues harvested from the mice 1 day and 4 weeks after injection were stained with hematoxylin and eosin and then examined by a pathologist. For hematological analysis, IO nanoparticles in PBS (100 μL) were intravenously injected into wild-type BALB/c mice at a dose of 5 mgFe/kg (n = 4–6 per group). PBS (100 μL) was only intravenously injected into wild-type BALB/c mice for a control group (n = 4–6). A 100 μL amount of blood was collected from the periorbital plexus under anesthesia through a heparinized capillary tube 1 day, 14 days, and 30 days after injection and transferred into EDTA-containing polypropylene microtubes (Becton Dickinson). Whole EDTA blood samples were analyzed in duplicate for hematology on a Hemavet 850FS Multi Species Hematology System (Drew Scientific) programmed with mouse hematology settings. For blood chemistries, IO nanoparticles in PBS (100 μL) were intravenously injected into wild-type BALB/c mice at a dose of 5 mgFe/kg (n = 4 or 5 per group). Up to 1 mL of blood was quickly withdrawn by cardiac puncture under anesthesia using a 1 mL plastic syringe with a 25 gauge needle. The needle was removed from the heart, and then blood was emptied into a Microtainer serum separator tube (Becton Dickinson) with no anticoagulant. Blood was allowed to clot 3 to 6 h at room temperature, then spun in the tube 5 min at 7000 rcf. Serum was removed and placed into a ~0.5 mL tube. For the first panel, 165 μL of sample was analyzed for bicarbonate, chloride, sodium, potassium, calcium, phosphorus, total protein, albumin, direct bilirubin, and total bilirubin analysis. For the second panel, 135 μL of serum was analyzed for glucose, BUN, creatinine, AST (SGOT), ALT (SGPT), and alkaline phosphatase analysis.

Statistical Analysis. Student's t-test (two-tailed, unpaired) was performed between monodisperse IO nanoparticles and control Feridex nanoparticles (Figures 2 and S1) or PBS (Figures 4 and S2).

Conflict of Interest: The authors declare no competing financial interest.

Acknowledgment. The authors thank E. Ruoslahti of the Sanford-Burnham Medical Research Institute for biological and animal experimental assistance and for helpful discussions, N. Varki of the Moores UCSD Cancer Center for performing the histological analyses, and the National Center for Microscopy and Imaging Research at UCSD for use of the transmission electron microscope. This work was supported by the National R&D Program for Cancer Control, Ministry for Health and Welfare, Republic of Korea, through grant no. 1220070 and the National Cancer Institute of the National Institutes of Health, USA, through grant no. 5-R01-CA124427 (BRP).

Supporting Information Available: Supplementary figures. This material is available free of charge *via* the Internet at http://pubs.acs.org.

REFERENCES AND NOTES

1. Weissleder, R.; Bogdanov, A.; Neuwelt, E. A.; Papisov, M. Long-Circulating Iron Oxide for MR Imaging. *Adv. Drug Delivery Rev.* **1995**, *16*, 321–334.
2. Corot, C.; Robert, P.; Idée, J.-M.; Port, M. Recent Advances in Iron Oxide Nanocrystal Technology for Medical Imaging. *Adv. Drug Delivery Rev.* **2006**, *58*, 1471–1504.
3. Jun, Y. W.; Seo, J. W.; Cheon, A. Nanoscaling Laws of Magnetic Nanoparticles and Their Applicabilities in Biomedical Sciences. *Acc. Chem. Res.* **2008**, *41*, 179–189.
4. Ros, P. R.; Freeny, P. C.; Harms, S. E.; Seltzer, S. E.; Davis, P. L.; Chan, T. W.; Stillman, A. E.; Muroff, L. R.; Runge, V. M.; Nissenbaum, M. A. Hepatic MR Imaging with Ferumoxides: A Multicenter Clinical Trial of the Safety and Efficacy in the Detection of Focal Hepatic Lesions. *Radiology* **1996**, *196*, 481–488.
5. Hyeon, T.; Lee, S. S.; Park, J.; Chung, Y.; Na, H. B. Synthesis of Highly Crystalline and Monodisperse Maghemite Nanocrystallites without a Size-Selection Process. *J. Am. Chem. Soc.* **2001**, *123*, 12798–12801.
6. Sun, S.; Zeng, H. Size-Controlled Synthesis of Magnetite Nanoparticles. *J. Am. Chem. Soc.* **2002**, *124*, 8204–8205.
7. Park, J.; An, K.; Hwang, Y.; Park, J.-G.; Noh, H.-J.; Kim, J.-Y.; Park, J.-H.; Hwang, N.-M.; Hyeon, T. Ultra-Large-Scale Syntheses of Monodisperse Nanocrystals. *Nat. Mater.* **2004**, *3*, 891–895.
8. Park, J.; Lee, E.; Hwang, N. M.; Kang, M. S.; Kim, S. C.; Hwang, Y.; Park, J. G.; Noh, H. J.; Kini, J. Y.; Park, J. H.; *et al.* One-Nanometer-Scale Size-Controlled Synthesis of Monodisperse Magnetic Iron Oxide Nanoparticles. *Angew. Chem., Int. Ed.* **2005**, *44*, 2872–2877.
9. Jun, Y. W.; Huh, Y. M.; Choi, J. S.; Lee, J. H.; Song, H. T.; Kim, S.; Yoon, S.; Kim, K. S.; Shin, J. S.; Suh, J. S.; *et al.* Nanoscale Size Effect of Magnetic Nanocrystals and Their Utilization for Cancer Diagnosis *via* Magnetic Resonance Imaging. *J. Am. Chem. Soc.* **2005**, *127*, 5732–5733.
10. Park, J.-H.; Maltzahn, G. v.; Zhang, L.; Schwartz, M. P.; Ruoslahti, E.; Bhatia, S. N. Sailor, M. J., Magnetic Iron Oxide Nanoworms for Tumor Targeting and Imaging. *Adv. Mater.* **2008**, *20*, 1630–1635.
11. Sun, S.; Zeng, H.; Robinson, D. B.; Raoux, S.; Rice, P. M.; Wang, S. X.; Li, G. Monodisperse MFe_2O_4 (M = Fe, Co, Mn) Nanoparticles. *J. Am. Chem. Soc.* **2004**, *126*, 273–279.

12. Lee, J. H.; Huh, Y. M.; Jun, Y.; Seo, J.; Jang, J.; Song, H. T.; Kim, S.; Cho, E. J.; Yoon, H. G.; Suh, J. S.; *et al*. Artificially Engineered Magnetic Nanoparticles for Ultrasensitive Molecular Imaging. *Nat. Med.* **2007**, *13*, 95–99.
13. Yang, J.; Gunn, J.; Dave, S. R.; Zhang, M.; Wang, Y. A.; Gao, X. Ultrasensitive Detection and Molecular Imaging with Magnetic Nanoparticles. *Analyst* **2008**, *133*, 154–160.
14. Jain, T. K.; Reddy, M. K.; Morales, M. A.; Leslie-Pelecky, D. L.; Labhasetwar, V. Biodistribution, Clearance, and Biocompatibility of Iron Oxide Magnetic Nanoparticles in Rats. *Mol. Pharmaceutics* **2008**, *5*, 316–327.
15. Lee, P.-W.; Hsu, S.-H.; Wang, J.-J.; Tsai, J.-S.; Lin, K.-J.; Wey, S.-P.; Chen, F.-R.; Lai, C.-H.; Yen, T.-C.; Sung, H.-W. The Characteristics, Biodistribution, Magnetic Resonance Imaging and Biodegradability of Superparamagnetic Core-Shell Nanoparticles. *Biomaterials* **2010**, *31*, 1316–1324.
16. Dubertret, B.; Skourides, P.; Norris, D. J.; Noireaux, V.; Brivanlou, A. H.; Libchaber, A. *In Vivo* Imaging of Quantum Dots Encapsulated in Phospholipid Micelles. *Science* **2002**, *298*, 1759–1762.
17. Park, J.-H.; von Maltzahn, G.; Ruoslahti, E.; Bhatia, S. N.; Sailor, M. J. Micellar Hybrid Nanoparticles for Simultaneous Magnetofluorescent Imaging and Drug Delivery. *Angew. Chem., Int. Ed.* **2008**, *47*, 7284–7288.
18. Torchilin, V. P. Structure and Design of Polymeric Surfactant-Based Drug Delivery Systems. *J. Controlled Release* **2001**, *73*, 137–172.
19. Weissleder, R.; Stark, D. D.; Engelstad, B. L.; Bacon, B. A.; Compton, C. C.; White, D. L.; Jacobs, P.; Lewis, J. Superparamagnetic Iron Oxide: Pharmacokinetics and Toxicity. *Am. J. Roentgenol.* **1989**, *152*, 167–173.
20. Pouliquen, D.; Jeune, J. J. L.; Perdrisot, R.; Ermias, A.; Jallet, P. Iron Oxide Nanoparticles for Use as an MRI Contrast Agent: Pharmacokinetics and Metabolism. *Magn. Reson. Imaging* **1991**, *9*, 275–283.
21. Briley-Saebo, K.; Bjørnerud, A.; Grant, D.; Ahlstrom, H.; Berg, T.; Kindberg, G. M. Hepatic Cellular Distribution and Degradation of Iron Oxide Nanoparticles Following Single Intravenous Injection in Rats: Implications for Magnetic Resonance Imaging. *Cell Tissue Res.* **2004**, *316*, 315–323.
22. Levy, M.; Luciani, N.; Alloyeau, D.; Elgrabli, D.; Deveaux, V.; Pechoux, C.; Chat, S.; Wang, G.; Vats, N.; Gendron, F.; *et al*. Long Term *in Vivo* Biotransformation of Iron Oxide Nanoparticles. *Biomaterials* **2011**, *32*, 3988–3999.
23. Na, H. B.; Lee, J. H.; An, K. J.; Park, Y. I.; Park, M.; Lee, I. S.; Nam, D. H.; Kim, S. T.; Kim, S. H.; Kim, S. W.; *et al*. Development of a T-1 Contrast Agent for Magnetic Resonance Imaging Using MnO Nanoparticles. *Angew. Chem., Int. Ed.* **2007**, *46*, 5397–5401.
24. Perrault, S. D.; Walkey, C.; Jennings, T.; Fischer, H. C.; Chan, W. C. W. Mediating Tumor Homing Efficiency of Nanoparticles through Design. *Nano Lett.* **2009**, *2009*, 1909–1915.
25. Moghimi, S. M.; Hunter, A. C.; Murray, J. C. Long-Circulating and Target-Specific Nanoparticles: Theory to Practice. *Pharm. Rev* **2001**, *53*, 283–318.
26. Park, J.-H.; Maltzahn, G. v.; Zhang, L.; Derfus, A. M.; Simberg, D.; Harris, T. J.; Ruoslahti, E.; Bhatia, S. N.; Sailor, M. J. Systematic Surface Engineering of Magnetic Nanoworms for *in Vivo* Tumor Targeting. *Small* **2009**, *5*, 694–700.
27. Chena, Z. P.; Zhang, Y.; Zhang, S.; Xia, J. G.; Liu, J. W.; Xu, K.; Gua, N. Preparation and Characterization of Water-Soluble Monodisperse Magnetic Iron Oxide Nanoparticles *via* Surface Double-Exchange with DMSA. *Colloids and Surfaces A: Physicochem. Eng. Aspects* **2008**, *316*, 210–216.
28. Wunderbaldinger, P.; Josephson, L.; Weissleder, R. Tat Peptide Directs Enhanced Clearance and Hepatic Permeability of Magnetic Nanoparticles. *Bioconjugate Chem.* **2002**, *13*, 264–268.